Skew-Grid Dichroic Plate with Rectangular Apertures for Use on a Ka-band Beam Waveguide Antenna

J. C. Chen, P. H. Stanton, and H. F. Reilly

Jet Propulsion Laboratory
4800 Oak Grove Drive, Pasadena
California 91109, U.S.A.

The first Ka-band Deep Space Network downlink demonstration was recently carried out by the Ka-Band Link Experiment (KABLE) in association with the Mars Observer spacecraft. In order to support the mission, a dichroic plate was required in the DSS-13 beam waveguide antenna to allow simultaneous X- and Ka-band dual-frequency operation. An X/Ka/KABLE dichroic plate was designed to transmit a future Ka-band downlink (31.8-32.3 GHz), future Ka-band uplink (34.2-34.7 GHz), and KABLE downlink frequency (33.6-33.8 GHz), while reflecting X-band (7.1-8.6 GHz). A computer program was developed for the analysis of a dichroic plate with rectangular apertures using the mode-matching method. The plate was then fabricated and tested. The reflection, group delay, and noise temperature in the antenna system due to the dichroic plate were measured. The experimental results show good agreement with theoretical predictions.

I. Introduction

The Deep Space Network has a need for a dichroic plate that will simultaneously receive X- and Ka-bands on a beam waveguide antenna where an ultra-low-noise receiver is used at Ka-band (Figure 1). The plate is required to pass a circularly polarized wave at (1) the Ka-band downlink (31.8-32.3 GHz) with a low insertion loss (as low as 0.04 dB), (2) a high-power Ka-band uplink (34.2-34.7 GHz), and (3) the Mars Observer

spacecraft Ka-band Link Experiment (KABLE) frequency (33.6-33.8 GHz), while at same time reflecting the X-band downlink (8.4-8.5 GHz). A thin dichroic plate with apertures or patches is not mechanically suitable for these requirements; therefore, a thick metallic plate with rectangular apertures was designed and fabricated (Figure 2). Mechanical constraints also require an oblique angle of incidence, while bandwidth considerations dictate the use of a skew grid (Figure 3).

II. Analysis

The analysis of a thick frequency selective surface with rectangular apertures is done in the following steps. First, a model of a half-space infinite array is used [1]. A complete set of basis functions with unknown coefficients is developed for the waveguide region (waveguide modes) and for the free space region (Floquet modes) in order to represent the electromagnetic fields [2]. Next, the boundary conditions are applied at the interface between these two regions. The method of moments is used to compute the unknown mode coefficients [3,4]. The scattering matrix of the half-space infinite array is then calculated. The reference plane of the scattering matrix is moved half a plate thickness in the negative z-direction. Finally, a frequency selective surface of finite thickness is synthesized by positioning two plates of half-thickness back-to-back. The total scattering matrix is obtained by cascading the scattering matrices of the two half-space infinite arrays.

A. Floquet Modes and Waveguide Modes

The analysis starts with an infinite array in half space (Figure 4a) consisting of a free space region ($z > 0$) and a waveguide region ($z < 0$). The electromagnetic fields in each region are represented by a set of orthonormal basis functions, Floquet and waveguide modes respectively, which satisfy Maxwell's equations. In the free space region (region I, $z > 0$), the electromagnetic field is represented as

$$\overline{E}_I(x,y,z) = \sum_{i=1}^{NFL}[A_{I_i}\exp(j\Gamma_i z) + B_{I_i}\exp(-j\Gamma_i z)]\overline{\Psi}_j(x,y)$$

$$\overline{H}_I(x,y,z) = \sum_{i=1}^{NFL}\frac{1}{Y_i}[A_{I_i}\exp(j\Gamma_i z) - B_{I_i}\exp(-j\Gamma_i z)]\overline{\Psi}_j(x,y)$$

where NFL is the number of Floquet modes, and A_{I_j} and B_{I_j} are the magnitudes of the incident and scattered Floquet modes. The Floquet modes Ψ_i (x, y) stands for $\overline{\Psi}_{mn}^{TEorTM}(x,y)$, which is either TE or TM mode with order mn [1]. In the waveguide region (region II, $z < 0$), the electromagnetic field is represented as

$$\overline{E}_{II}(x,y,z) = \sum_{j=1}^{NWG}[A_{II_j}\exp(-j\gamma_j z) + B_{II_j}\exp(j\gamma_j z)]\overline{\Phi}_j(x,y)$$

$$\overline{H}_{II}(x,y,z) = \sum_{j=1}^{NWG} -\frac{1}{y_j}[A_{II_j}\exp(-j\gamma_j z) - B_{II_j}\exp(j\gamma_j z)]\overline{\Phi}_j(x,y)$$

where NWG is the number of waveguide modes, and A_{II_j} and B_{II_j} are the magnitudes of the incident and reflected waveguide modes. $\overline{\Phi}_j(x,y)$ stands for $\overline{\Phi}_{mn}^{TEorTM}(x,y)$, which is either TE or TM mode with order mn [5].

The periodicity of the infinite array simplifies the analysis to a study of a single equivalent element. If the problem did not have this periodicity then the mutual coupling would have to be evaluated element by element, increasing the complexity of the computation.

B. Boundary Conditions and Method of Moments

The electromagnetic field in the free space is expressed as a sum of incident and reflected Floquet modes, while in the waveguide region as a sum of incident and reflected waveguide modes. Boundary conditions are applied at the interface between two regions; i.e., the transverse electric and magnetic field must be continuous across the junction at $z=0$:

$$\overline{E}_{I_T} = \overline{E}_{II_T}$$
$$\overline{H}_{I_T} = \overline{H}_{II_T}$$

This leads to an integral equation for the unknown transverse electric field at the boundary. The infinite array scattering problem then becomes similar to a two-region waveguide problem.

The method of moments is used to transform the integral equation into a matrix equation suitable for evaluation on a digital computer. Solving the set of linear equations gives the unknown mode coefficients in both regions. The time required for filling the matrix depends on the number of Floquet and waveguide modes used. The number of waveguide modes and Floquet modes used in the program can be increased by the user to ensure convergence of the solution [6,7].

C. Scattering Matrix for the Waveguide Array

The characteristics of the infinite array referenced to $z = 0$ are represented by a scattering matrix [$S^{(0)}$], which contains the transmission and reflection information for the free space to waveguide junction. [$S^{(0)}$] is composed of four matrices :

$$\left[S^{(0)}\right] = \begin{bmatrix} \left[S_{11}^{(0)}\right] & \left[S_{12}^{(0)}\right] \\ \left[S_{21}^{(0)}\right] & \left[S_{22}^{(0)}\right] \end{bmatrix}$$

where $\left[S_{11}^{(0)}\right]$, $\left[S_{12}^{(0)}\right]$, $\left[S_{21}^{(0)}\right]$, and $\left[S_{22}^{(0)}\right]$ are matrices with 1 representing the free space region and 2 the waveguide region. The size of matrix $\left[S_{11}^{(0)}\right]$ is 2 by 2, $\left[S_{22}^{(0)}\right]$ is NWG by NWG, $\left[S_{12}^{(0)}\right]$ is 2 by NWG, $\left[S_{21}^{(0)}\right]$ is

NWG by 2, and NWG is the number of waveguide modes used. For example,

$$\left[S_{21}^{(0)}\right]=\begin{bmatrix} S_{21}^{(0)}(1,1) & S_{21}^{(0)}(1,2) \\ S_{21}^{(0)}(2,1) & S_{21}^{(0)}(2,2) \\ \vdots & \vdots \\ S_{21}^{(0)}(NWG,1) & S_{21}^{(0)}(NWG,2) \end{bmatrix}$$

where $S_{21}^{(0)}(k,l)$ are complex numbers.

For the incident TE_{00} and TM_{00} Floquet modes, whose the coefficients are contained in vector $\bar{a}_1$, and an arbitrary set of incident waveguide modes, whose the coefficients are contained in vector $\bar{a}_2$, the reflected modes $\bar{b}_1$ and $\bar{b}_2$ are determined by the following set of equations (Figure 4a) :

$$\bar{b}_1 = \left[S_{11}^{(0)}\right]\bar{a}_1 + \left[S_{12}^{(0)}\right]\bar{a}_2^{(0)}$$
$$\bar{b}_1^{(0)} = \left[S_{21}^{(0)}\right]\bar{a}_1 + \left[S_{22}^{(0)}\right]\bar{a}_2^{(0)}$$

Moving the reference plane in the waveguide region from $z=0$ to $z=-t/2$ (Figure 4b), where t is the thickness of the plate, the elements of the new scattering matrix $[S^{(1)}]$ become:

$$S_{11}^{(1)}(k,l) = S_{11}^{(0)}(k,l)$$
$$S_{12}^{(1)}(k,l) = S_{12}^{(0)}(k,l)\exp[-j\gamma_l \frac{t}{2}]$$
$$S_{21}^{(1)}(k,l) = S_{21}^{(0)}(k,l)\exp[-j\gamma_k \frac{t}{2}]$$
$$S_{22}^{(1)}(k,l) = S_{22}^{(0)}(k,l)\exp[-j\gamma_k \frac{t}{2}]\exp[-j\gamma_l \frac{t}{2}]$$

where γ_k and γ_l are the propagation constants of waveguide mode k and mode l, respectively.

D. Scattering Matrix for the Thick FSS

Scattering by a frequency selective surface with finite thickness can be analyzed by considering two infinite array problems. The scattering matrix with reference to $z = -t/2$ for regions I and II is [S $^{(1)}$], while the scattering matrix with reference to $z = -t/2$ for regions III and IV is [S $^{(2)}$], which is the transpose matrix of [S $^{(1)}$] (Figure 5a) :

$$[S_{11}^{(2)}] = [S_{22}^{(1)}]$$
$$[S_{12}^{(2)}] = [S_{21}^{(1)}]$$
$$[S_{21}^{(2)}] = [S_{12}^{(1)}]$$
$$[S_{22}^{(2)}] = [S_{11}^{(1)}]$$

The scattering matrix [S] for the finite thickness plate is determined by cascading these two matrices (Figure 5b).

A computer program was written based on the analysis above. The cell size, skew angle, aperture size, dielectrics in the apertures, and the plate thickness are the input variables in the software. The program calculates the scattering matrix, including the magnitude and the phase of the transmission and reflection coefficients.

III. X/Ka/KABLE Dichroic Plate Design

The X/Ka/KABLE dichroic plate was designed using the thick frequency selective surface program based on the mode-matching method described above [8]. The cell size and pattern (D_x, D_y and Ω), the aperture size (A_x, A_y), and the thickness of the plate (t) are adjusted to meet the requirements. The angle of incidence is θ = 30.0 deg and ϕ = 0.0 deg (Figure 3). The aperture wall thickness is limited to a 0.203-mm (0.008-in.) minimum due to mechanical constraints. The dichroic plate design was optimized with the following priority (1) Ka-band downlink, (2) Ka-band uplink, and (3) KABLE frequencies.

The optimized design of the X/Ka/KABLE dichroic plate employs a rectangular aperture of size 5.080 mm (0.200 in., A_x) by 5.156 mm (0.203 in., A_y); cell size 6.198 mm (0.244 in., D_x) by 5.359 mm (0.211 in., D_y) with a 60-deg skew angle (Ω); and plate thickness 9.271 mm (0.365 in., t) (Figure 6a). The reflection loss is about 0.007 dB at 32 GHz, 0.078 dB at 34.5 GHz, and 0.103 dB at 33.7 GHz [8]. The phase difference between the two linear polarizations is 3.4 deg to 4.0 deg at the Ka-band downlink, 1.8 deg to 3.8 deg at uplink, and -0.2 deg to 0.5 deg at KABLE [8]. The phase shift can be corrected by adjusting the polarizer. The overall size of the plate is 765.048 mm-by-647.700 mm (30.12 in.-by-25.50 in.) with the elliptical perforated area 561.848 mm-by-444.50 mm (22.12 in.-by-17.5 in.) (Figure 6b).

IV. Grating Lobe Study

Generally, the angle of transmission is equal to the angle of incidence (principal direction). But for certain circumstances, higher order modes are excited and some of the transmitted power leaves at an angle other than the principal direction. These excited higher order modes are called grating lobes and are similar to the grating lobes in a phased array antenna. The conditions of the existence of a grating lobe depend on the angle of incidence, the frequency, and the size and skew angle of the cells on the plate. Since the incident wave is a horn pattern rather than a perfect plane wave, grating lobes may be generated by portions of the horn radiation that strike the plate at large angles of incidence.

The study of the grating lobe effects on a dichroic plate/feedhorn system is carried out in a series of steps. First, grating lobes that may be excited by a plane wave illumination are discussed. Next, expansion of a feedhorn pattern in terms of a group of plane waves traveling at different angles is described. Finally, the grating lobes that are excited by a horn pattern are determined [9].

A. Structure Dependence

For a certain angle of incidence φ, as θ is increased beyond some critical value ($\geq \theta_g$), grating lobes may be excited. This is predicted in

Figure 7, where the X-axis and Y-axis represent the angles φ and θ, respectively. For example, the point (0,54) on the scallop-shaped curve for 34.7 GHz in Figure 7 indicates that when φ =0.0 deg, grating lobes are generated for $\theta \geq 54.0$ deg for the given cell size of 6.1976 mm with a 60-deg skew angle (X/Ka/KABLE dichroic plate). The shape of a θ_g curve depends on the cell pattern. Also, the higher the frequency, the smaller the θ_g for a given cell size.

B. Horn Pattern Study

The far-field horn pattern can be represented as a plane wave expansion, i.e., a group of plane waves traveling with different amplitudes at different angles. If the horn is placed at θ_0, φ_0, the different angles of incidence of these plane waves on the dichroic plate may be calculated through a coordinate transformation from the horn coordinate system to the dichroic plate coordinate system. The far-field horn pattern is assumed to be symmetric in φ. The concentric circular curves in the horn coordinate system are still concentric but not circular after being transformed to dichroic plate coordinate system for the case of horn pattern incidence on the dichroic plate at an oblique angle. Figure 7 shows the angle of incidence on a dichroic plate from a horn with a symmetric pattern placed at θ_0 = 30.0 deg, φ_0 = 0.0 deg. Each curve is for a constant θ_h in the horn coordinate system. For a 26-dB horn, θ_h = 12.0 deg is about -18 dB with respect to the on-axis peak and θ_h = 14.0 deg is about -21 dB.

C. Excitation of Grating Lobes by Horn Pattern

The grating lobe plot and the horn pattern plot need to overlapped to determine the severity of the grating lobe problem for a given horn/dichroic plate geometry. For the X/Ka/KABLE dichroic plate, the horn is tilted 30.0 deg from normal at φ = 0.0 deg. The θ_g curve for 33.8 GHz (the high end of the KABLE frequency band) intersects with $\theta_h > 16.0$ deg curve, which is equivalent to 24 dB below the radiation peak, while the θ_g curve for 34.7 GHz (the high end of the Ka-band uplink) intersects partially with the θ_h =14.0 deg contour, which is equivalent to 21 dB below the radiation peak. Since the power at the angle of incidence where the grating lobes may be generated is very low (below 21 dB from the horn

radiation peak), grating lobe excitation is not a serious problem for the X/Ka/KABLE dichroic plate design.

V. Fabrication

The dichroic plate is made of copper for low conductivity loss. A tolerance study indicated that a ±0.0254-mm (±0.001-in.) tolerance on the dimensions of the apertures was acceptable in order to meet the RF requirements (Table 1). The plate was first drilled with an array of circular holes, then each hole was cut into a rectangular hole with a wire electrical discharge machine, producing higher accuracy and sharper rectangular corners compared to conventional machining methods. The walls of the rectangular apertures (waveguides) were then surface-treated with an Extrude Hone Process. In the Extrude Hone Process, two vertically opposed cylinders extrude abrasive media back and forth through the waveguide passages. The surface finish of the dichroic plate is 250μ mm (10μ in.). The average size of the finished apertures is 5.0607 mm-by-5.1265 mm (0.19924 in.-by-0.20183 in.) with 0.127-mm-radius (0.005-in-radius) corners according to JPL fabrication. The discrepancy of the apertures is thus 0.0193 mm (0.00076 in.) and 0.0297 mm (0.00117 in.), which is within the allowable tolerance. A photograph of the X/Ka/KABLE dichroic plate is shown in Figure 2.

VI. Reflection and Group Delay

In the experimental measurement of the reflection and group delay, the alignment between the transmit horn, dichroic plate, and the receiving horn is very important. There are two kinds of experimental setups: the reflection setup for determining the reflection coefficients, especially the resonant frequencies (Figure 8a), and the transmission setup for measuring the group delay (Figure 8b). Both experiments were performed using an HP 8510C Network Analyzer. The reflection of the dichroic plate at 30 deg from the normal direction was measured from 31 to 36 GHz. The measured and calculated reflection coefficients for TE and TM polarizations are shown in Figures 9 and 10. There are two resonant frequencies between 31 and 36 GHz for both the TE and TM polarization.

The resonant frequencies of the dichroic plate are within 0.04 to 0.36% of the predicted values (Table 2). The combined transmitted power for TE and TM polarizations is shown in Figure 11.

The group delay of the dichroic plate was measured using the transmission experiment setup. The calculated and the measured group delay versus frequency are shown in Figures 12 and 13. The group delay is 0.074 to 0.115 ns from 31.8 to 34.7 GHz for TE and TM polarizations. The group delay is about 0.002 ns higher than predicted (Table 3).

VII. Noise Temperature

In the antenna system the dichroic plate is illuminated by a horn whose radiation pattern is considered to be a group of plane waves traveling with different amplitudes at different angles. These plane waves will not all strike the dichroic plate at the same angle. Since the dichroic plate is optimized for a 30-deg incident angle, the reflection is minimized on that angle. Therefore, the reflected power by the dichroic plate for horn illumination is larger than the reflection for pure plane wave incidence at 30 deg. The reflected power thus adds noise temperature to the antenna system. For example, if 0.01-dB reflected power sees a 300-K hot background, it will be equivalent to 0.67-K noise temperature.

In addition to the reflected energy from the horn pattern, the conductivity loss (I^2R loss) for rough surface contributes to the overall noise temperature in the beam waveguide system. The noise temperature, which includes the reflection for plane wave incidence and conductivity loss (assuming smooth surface), is calculated to be 1.34 K, 5.83 K and 7.57 K at 32.0 GHz (downlink), 34.5 GHz (uplink), and 33.7 GHz (KABLE), respectively. Measurements were made at the KABLE frequency of 33.7 GHz in the DSS-13 beam waveguide antenna using a corrugated horn. The measured noise temperature at 33.7 GHz was 11 K, which is 3.43 K higher than the calculation due to the effects described above.

VIII. Conclusion

The design of an X/Ka/KABLE dichroic plate has been presented. The theoretical and experimental results show good agreement in predicting the performance of the dichroic plate (Table 4). The X/Ka/KABLE dichroic plate is currently installed in the DSS-13 beam waveguide antenna at Goldstone, California (Figure 14) for use in the KABLE experiment and future Ka-band operation.

Acknowledgment

The authors would like to thank D. Hoppe and R. Hodges for technical discussions, and L. Epp for correcting a coding error in the program. The research described in this paper was carried out at the Jet Propulsion Laboratory, California Institute of Technology, under a contract with the National Aeronautics and Space Administration.

References

1. N. Amitay, V. Galindo, and C. P. Wu, Theory and Analysis of Phased Array Antennas, New York: Wiley-Interscience, 1972.

2. C. C. Chen, "Transmission Through a Conducting Screen Perforated Periodically with Apertures," IEEE Trans. Microwave Theory Tech., vol. MTT-18, no. 9, pp. 627-623, September 1970.

3. C. C. Chen, "Transmission of Microwaves through Perforated Flat Plates of Finite Thickness," IEEE Trans. Microwave Theory Tech., vol. MTT-21, no. 1, pp. 1-6, January 1973.

4. S. W. Lee, W. R. Jones, and J. J. Campbell, "Convergence of Numerical Solutions of Iris-Type Discontinuity Problems," IEEE Trans. Microwave Theory Tech., vol. MTT-19, no. 6, pp. 528-536, June 1971.

5. N. Marcuvitz, The Waveguide Handbook, New York, McGraw-Hill book Company, Inc., 1951.

6. R. Mittra, T. Itoh, and T. S. Li, "Analytical and Numerical Studies of the Relative Convergence Phenomenon Arising in the Solution of an Integral Equation by the Moment Method," IEEE Trans. Microwave Theory Tech., vol. MTT-20, no. 2, pp. 96-104, February 1972.

7. S. W. Lee, G. Zarrillo, and C. L. Law, 'Simple Formulas for Transmission Through Periodic Metal Grids or Plates," IEEE Trans. Antenna Propagat., vol. AP-30, no. 5, pp. 904-909, September 1982.

8. J. C. Chen, "Analysis of a Thick Dichroic Plate with Rectangular Holes at Arbitrary Angles of Incidence," TDA Progress Report 42-104, October-December 1990, Jet Propulsion Laboratory, Pasadena, California, February 15, 1991.

9. J. C. Chen, "X/Ka-Band Dichroic Plate Design and Grating Lobe Study," TDA Progress Report 42-105, January-March 1991, Jet Propulsion Laboratory, Pasadena, California, May 15, 1991.

Table 1. Tolerance study of aperture size for the X/Ka/KABLE dichroic plate

Freq., GHz	Pol.	Aperture size, mm				
		A_x=5.0800 A_y=5.1562	ΔA_x= -0.0254	ΔA_x= +0.0254	ΔA_y= -0.0254	ΔA_y= +0.0254
		Refl. loss, dB	ΔRefl. loss, dB	ΔRefl. loss, dB	ΔRefl. loss, dB	ΔRefl. loss, dB
32.3	TE	0.023	+0.002	+0.016	+0.003	–0.002
	TM	0.025	–0.001	+0.002	–0.015	+0.019
33.8	TE	0.007	+0.003	–0.004	+0.000	–0.001
	TM	0.199	–0.005	+0.004	+0.001	–0.003
34.7	TE	0.078	–0.017	+0.019	+0.002	–0.002
	TM	0.096	–0.002	+0.003	+0.009	–0.008

Table 2. Measured and calculated resonant frequencies of the X/Ka/KABLE dichroic plate (calculation based on 40 waveguide modes)

Polarization	Resonant Frequency	Measurement, GHz	Calculation, GHz	% Error
TE	1st	32.03125	32.05	0.06
TE	2nd	34.00625	34.08	0.22
TM	1st	32.15625	32.17	0.04
TM	2nd	35.95000	35.82	0.36

Table 3. Group delay of the X/Ka/KABLE dichroic plate for TE and TM polarizations

Ka-Band	Frequency, GHz	Group delay, ns					
		TE pol.			TM pol.		
		meas.	cal.	Δ	meas.	cal.	Δ
Downlink	31.8	0.115	0.114	0.001	0.111	0.111	0.000
	32.0	0.108	0.107	0.001	0.105	0.105	0.000
	32.3	0.100	0.101	0.001	0.099	0.099	0.000
KABLE	33.6	0.085	0.083	0.002	0.077	0.074	0.003
	33.7	0.085	0.083	0.002	0.076	0.073	0.003
	33.8	0.085	0.083	0.002	0.075	0.073	0.002
Uplink	34.2	0.085	0.083	0.002	0.075	0.072	0.003
	34.5	0.085	0.083	0.002	0.074	0.072	0.002
	34.7	0.084	0.082	0.002	0.075	0.072	0.003

Table 4. Performance of the X/Ka/KABLE dichroic plate for the DSS-13 beam waveguide antenna

Frequency	32.0 GHz (Downlink)		33.7 GHz (KABLE)		34.5 GHZ (Uplink)	
Characteristics	Cal.[a]	Meas.	Cal.[a]	Meas.	Cal.[a]	Meas.
Reflection loss, dB	0.007	0.006	0.103	0.096	0.078	0.089
Conductivity loss[b], dB	0.013 approx.	—	0.010 approx.	—	0.009 approx.	—
Ellipticity, dB	0.294	—	0.220	—	0.603	—
Group delay, ns	0.106	0.102	0.078	0.080	0.078	0.080
Noise temperature, K	1.34 min[c]	TBD[d]	7.57 min[c]	11	5.83 min[c]	NA[e]

a. Calculation is based on perfect plane wave incidence.
b. Conductivity loss is calculated for a dominant mode propagating in a rectangular waveguide of 5.16 mm-by-5.08 mm with length 9.27 mm. It does not include the effect of surface roughness.
c. Calculated noise temperature only includes the reflection loss and conductivity loss.
d. To be determined.
e. Not applicable.

Figure Titles

Figure 1. DSS13 34-m DSN beam waveguide antenna

Figure 2. Photograph of the X/Ka/KABLE dichroic plate

Figure 3. Geometry of a dichroic plate with rectangular apertures

Figure 4a. Half-space infinite array with reference plance z = 0

Figure 4b. Half-space infinite array with reference plance z = -t/2

Figure 5a. Half-space infinite array with reference plance z = -t/2 for reverse case

Figure 5b. Finite-thickness (t) plate is analyzed by considering two infinite array problems

Figure 6a. Dimensions of the X/Ka/KABLE dichroic plate

Figure 6b. Overall size of the X/Ka/KABLE dichroic plate

Figure 7. Excitation of grating lobes by the feedhorn pattern for the X/Ka/KABLE dichroic plate

Figure 8a. Experimental setup for reflection measurement

Figure 8b. Experimental setup for group delay measurement

Figure 9. Calculated and measured reflection coefficient vs. frequency for X/Ka/KABLE dichroic plate for TE polarizations

Figure 10. Calculated and measured reflection coefficient vs. frequency for X/Ka/KABLE dichroic plate for TM polarizations

Figure 11. Transmitted power for X/Ka/KABLE dichroic plate

Figure 12. Calculated and measured group delay vs. frequency for X/Ka/KABLE dichroic plate for TE polarizations

Figure 13. Calculated and measured group delay vs. frequency for X/Ka/KABLE dichroic plate for TM polarizations

Figure 14. The X/Ka/KABLE dichroic plate installed at the DSS-13 beam waveguide antenna

JPL 34-M DSN BEAM WAVEGUIDE ANTENNA

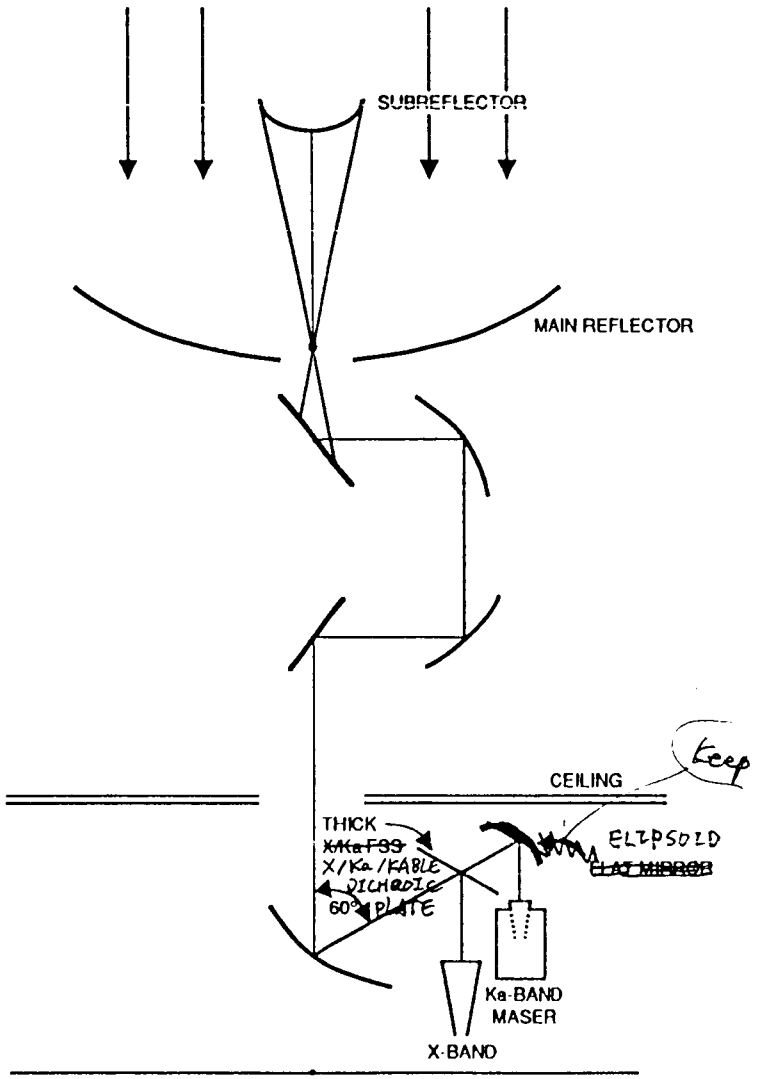

Figure 1

JCC
6/28/91

Figure 2. Photograph of X/Ka/KABLE dichroic plate

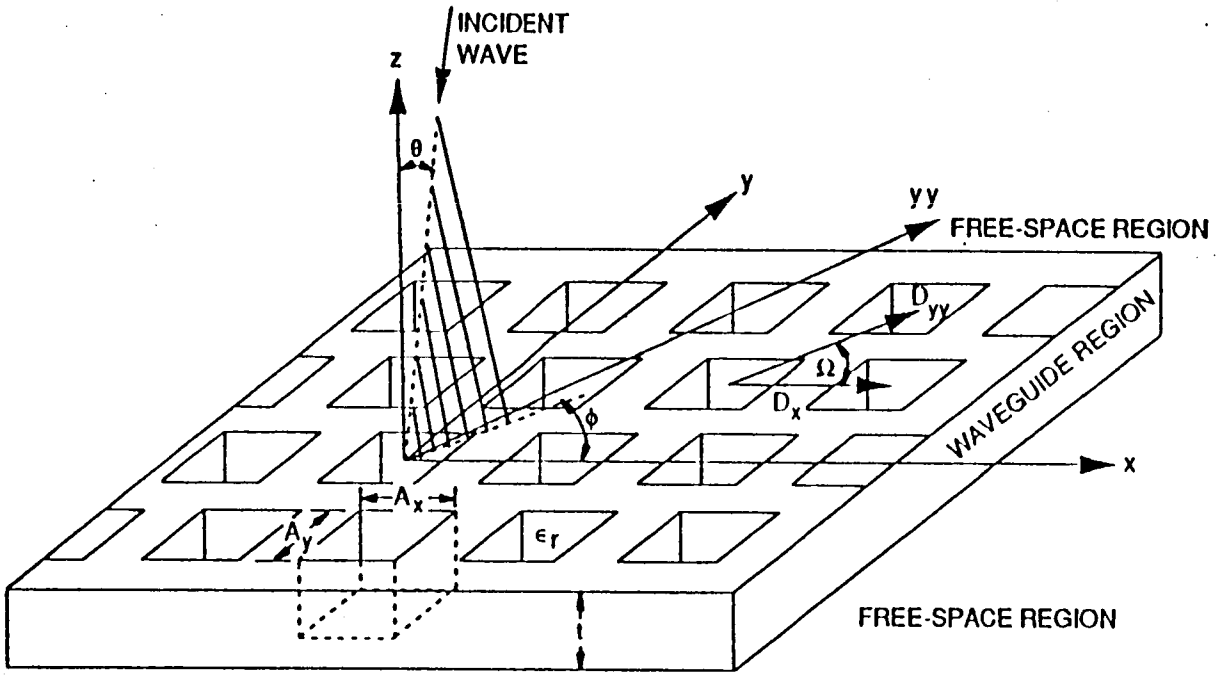
INCIDENT
WAVE
z
θ
y
yy
FREE-SPACE REGION
D_{yy}
Ω
D_x
ϕ
WAVEGUIDE REGION
x
A_x
A_y
ϵ_r
FREE-SPACE REGION

Fig. 3.

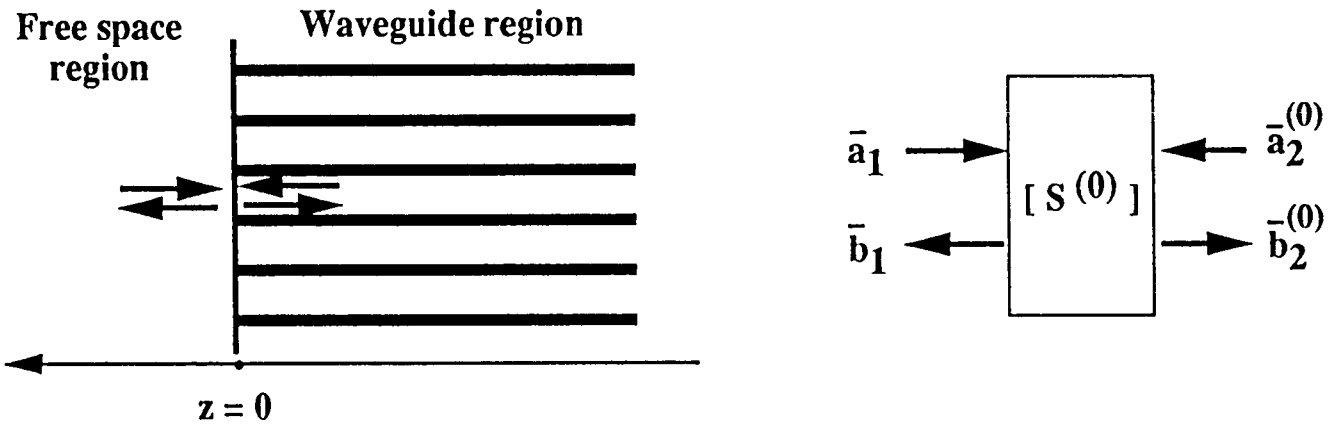

Fig. 2-a Half-space infinite array with reference plane z = 0.

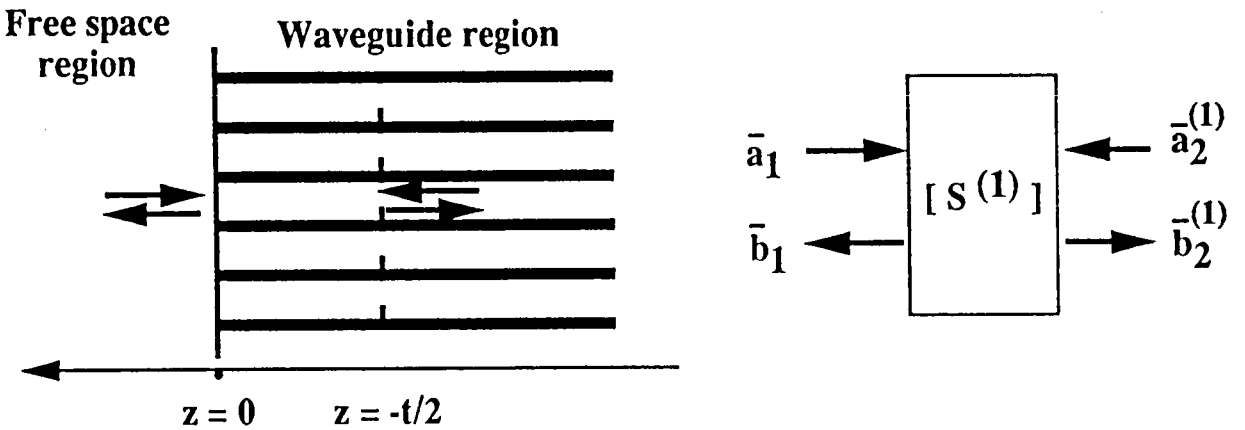

Fig. 2-b Half space infinte array with reference plane z = -t/2.

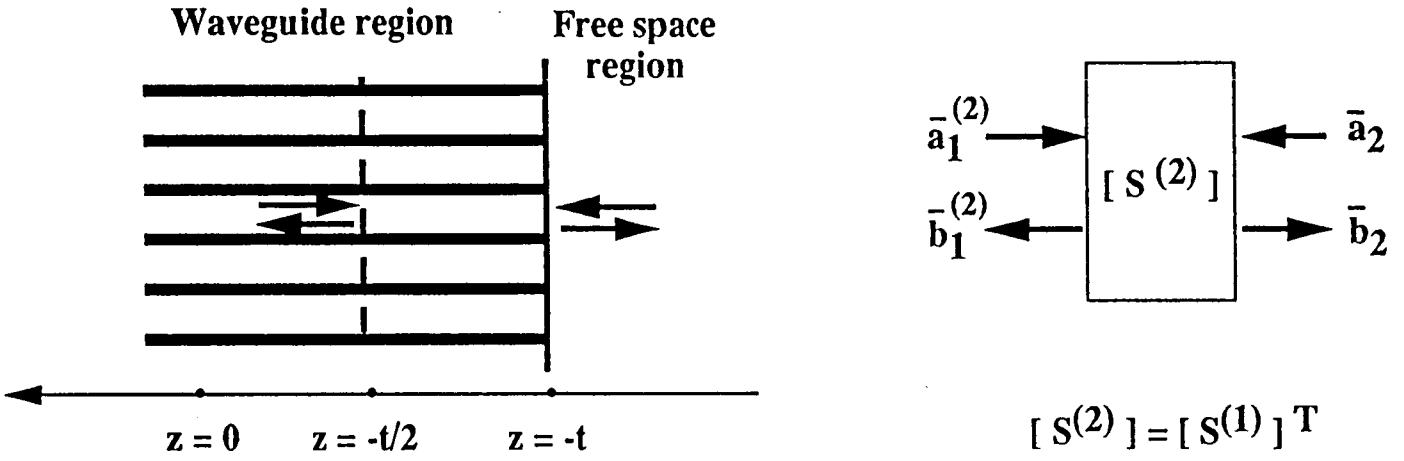

Fig. 3-a Half space infinite array with reference z = -t/2 for reverse case.

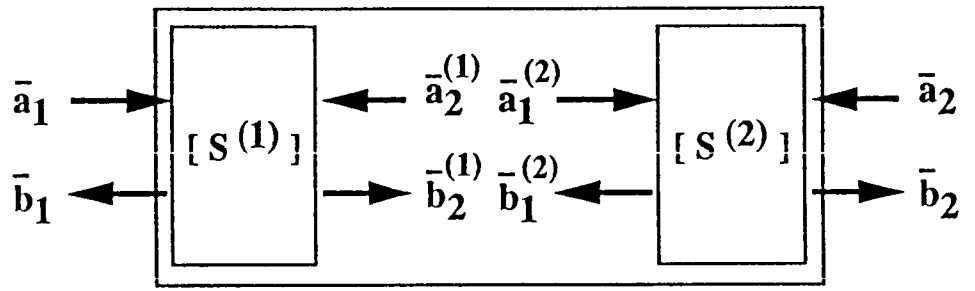

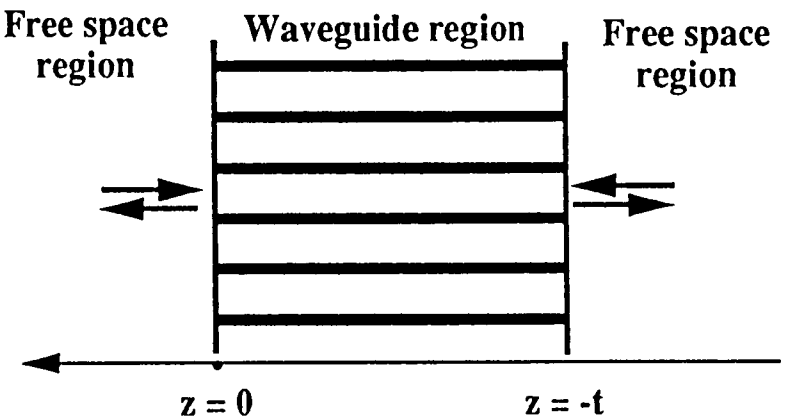

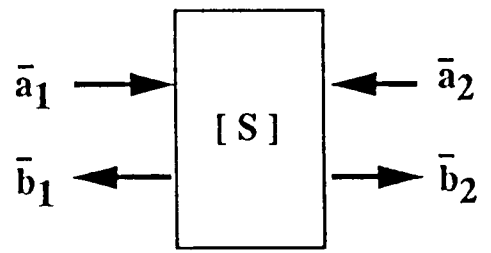

Fig. 3-b Finite-thickness (t) plate is analyzed by considering two infinite array problems.

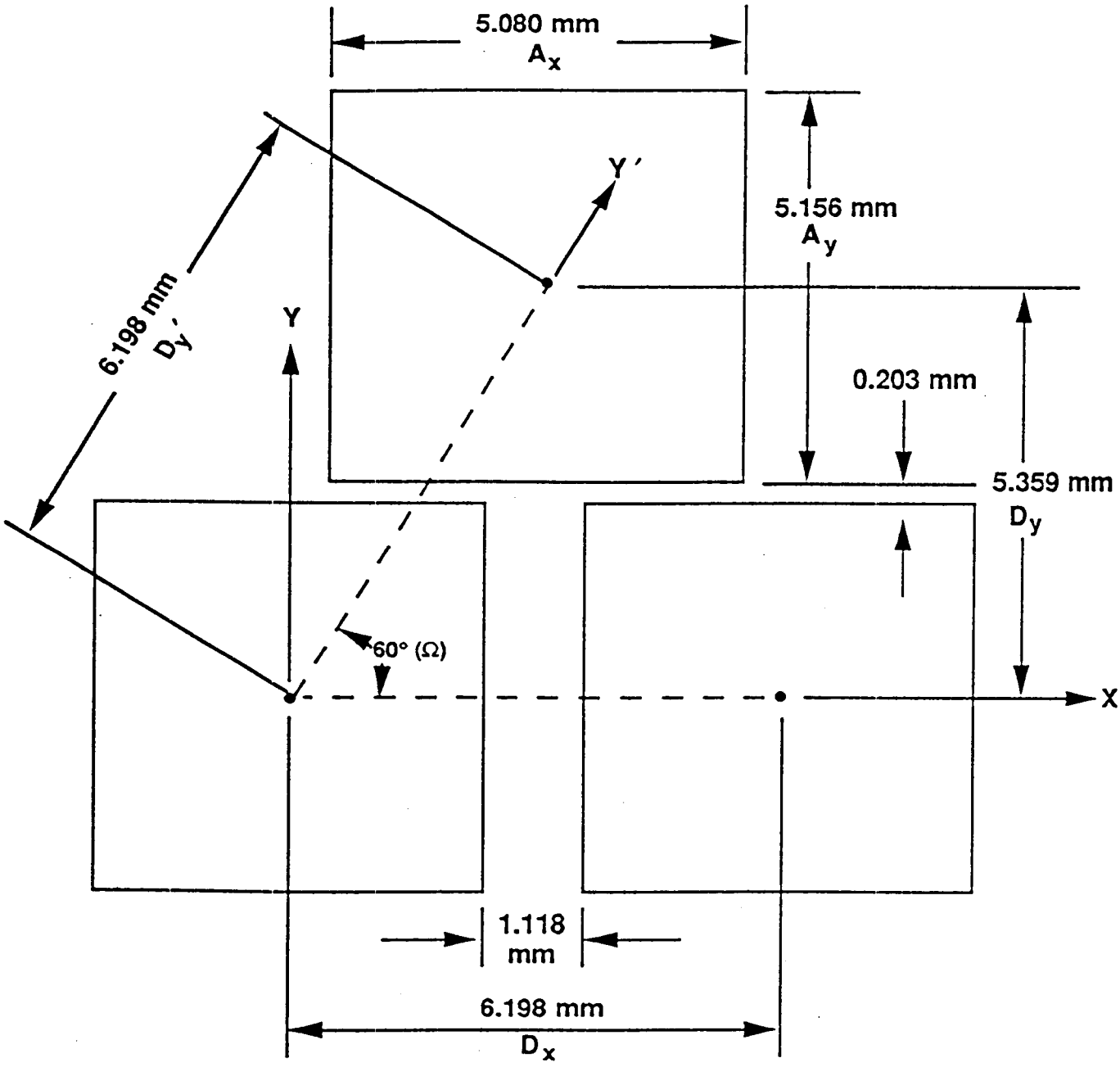

THICKNESS (t) = 9.271 mm

Figure 3a

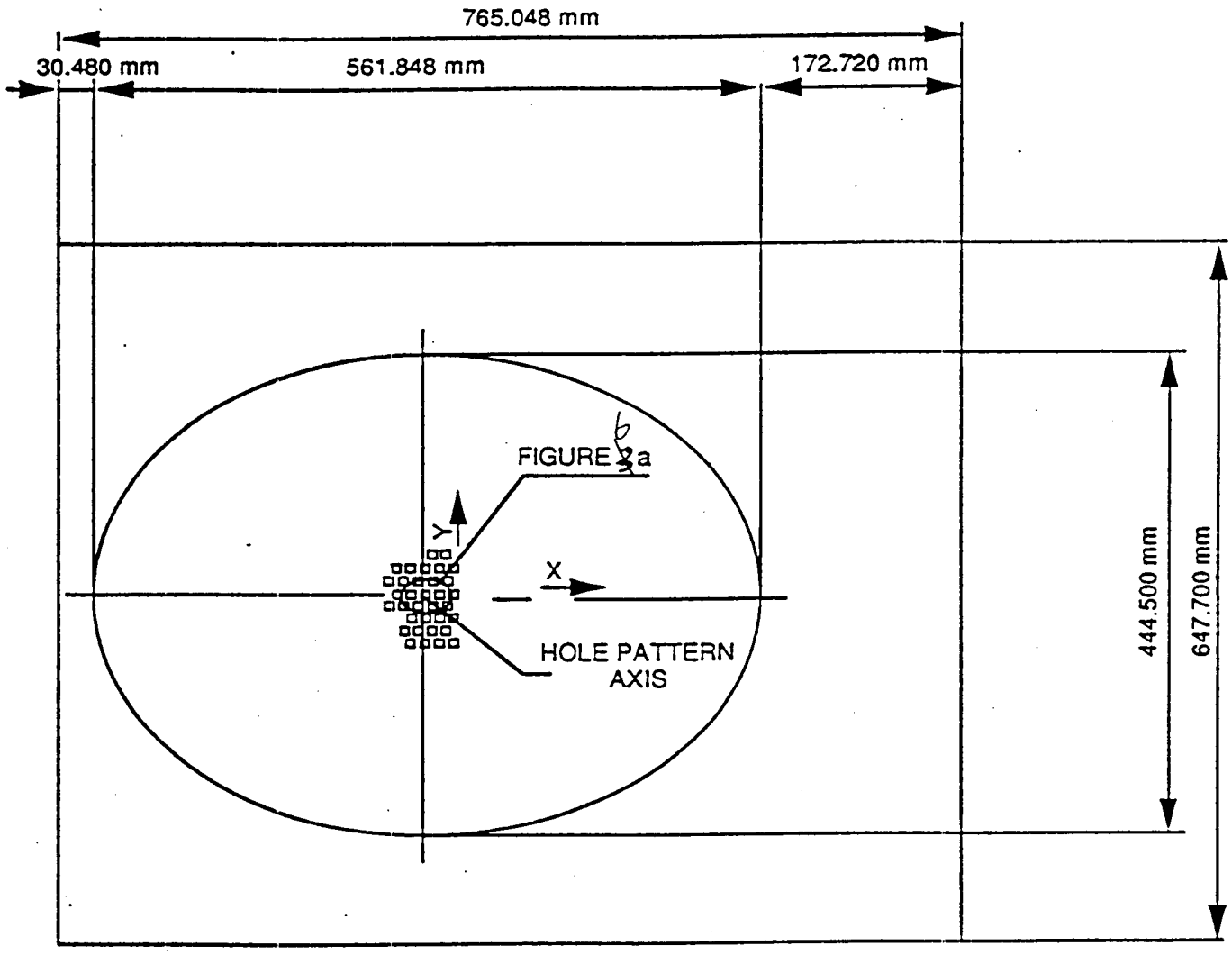
765.048 mm
30.480 mm
561.848 mm
172.720 mm
FIGURE 6a
Y
X
HOLE PATTERN
AXIS
444.500 mm
647.700 mm

Figure 6b

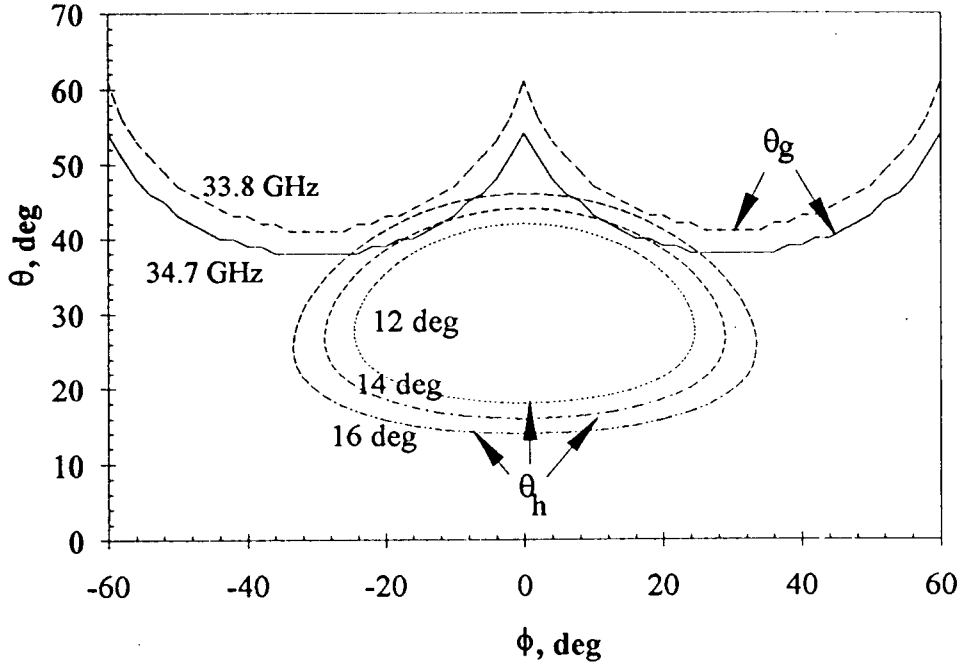
70
60
50
40
30
20
10
0
θ, deg
-60
-40
-20
0
20
40
60
ϕ, deg
33.8 GHz
34.7 GHz
θg
12 deg
14 deg
16 deg
θh

Figure 7

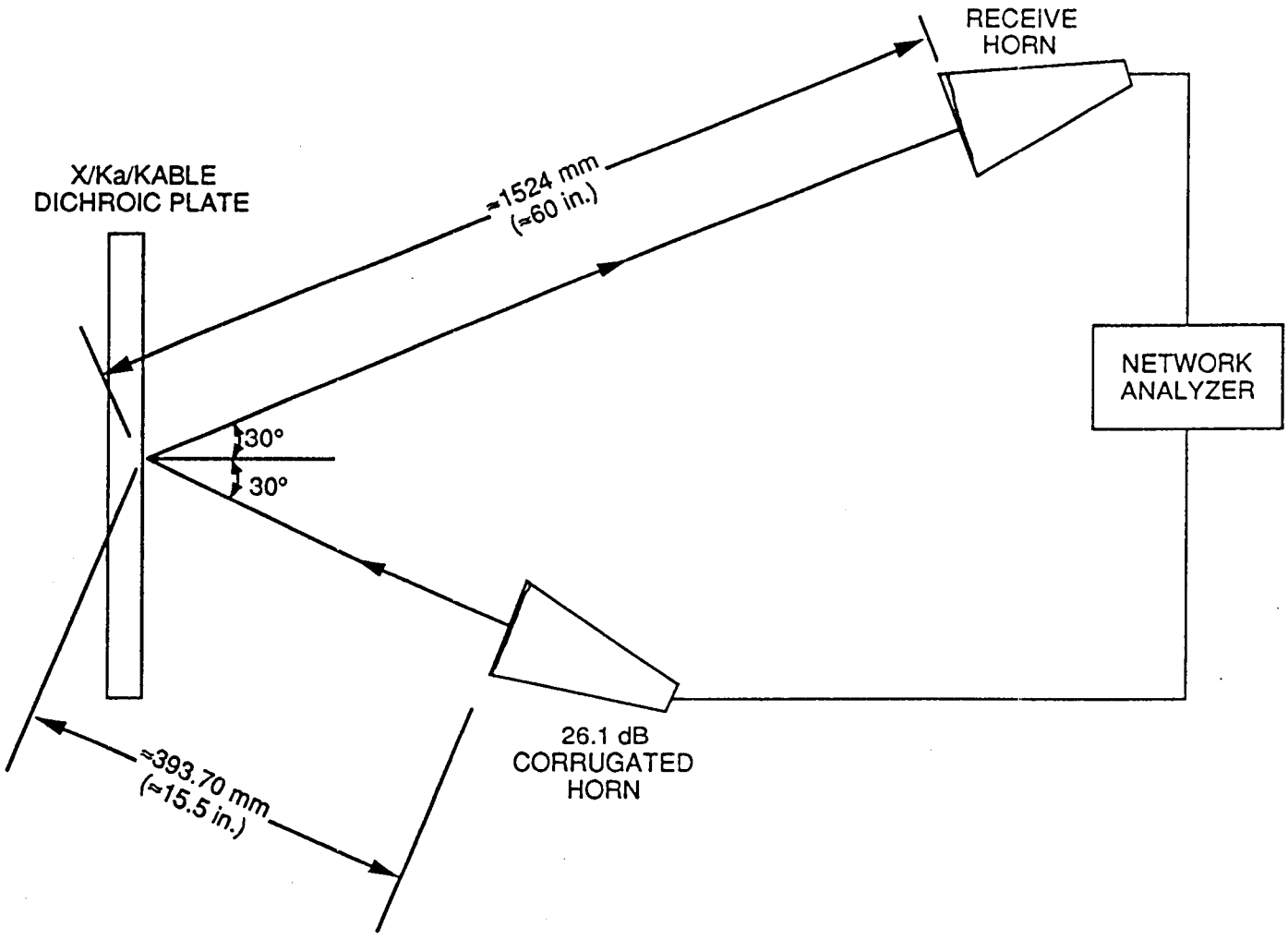
RECEIVE
HORN
X/Ka/KABLE
DICHROIC PLATE
≈1524 mm
(≈60 in.)
NETWORK
ANALYZER
30°
30°
26.1 dB
CORRUGATED
HORN
≈393.70 mm
(≈15.5 in.)

Figure 8a

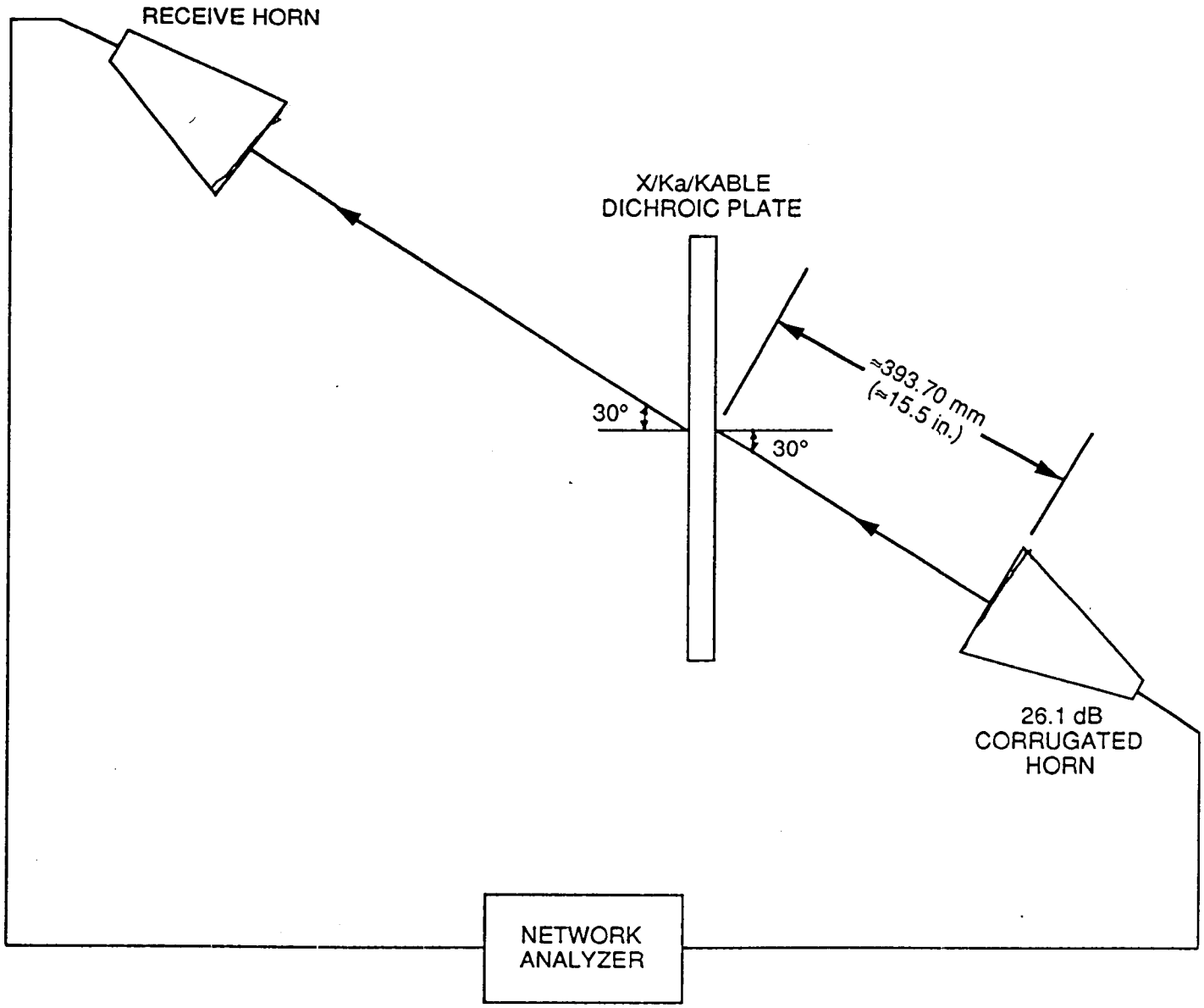
RECEIVE HORN
X/Ka/KABLE
DICHROIC PLATE
≈393.70 mm
(≈15.5 in.)
30°
30°
26.1 dB
CORRUGATED
HORN
NETWORK
ANALYZER

Figure 8b

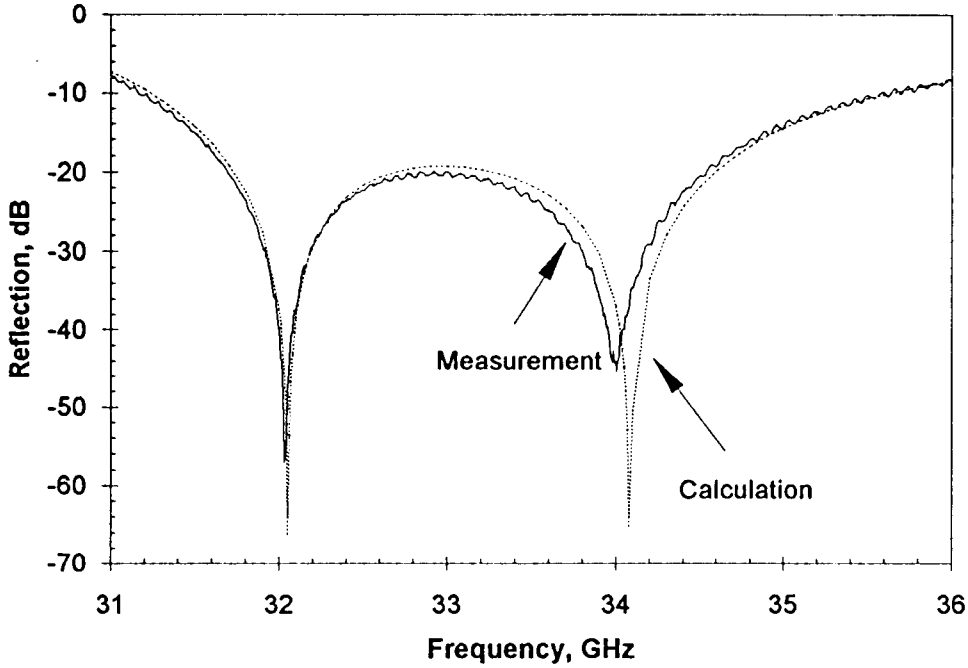
0
-10
-20
-30
-40
-50
-60
-70
Reflection, dB
31
32
33
34
35
36
Frequency, GHz
Measurement
Calculation

Figure 9

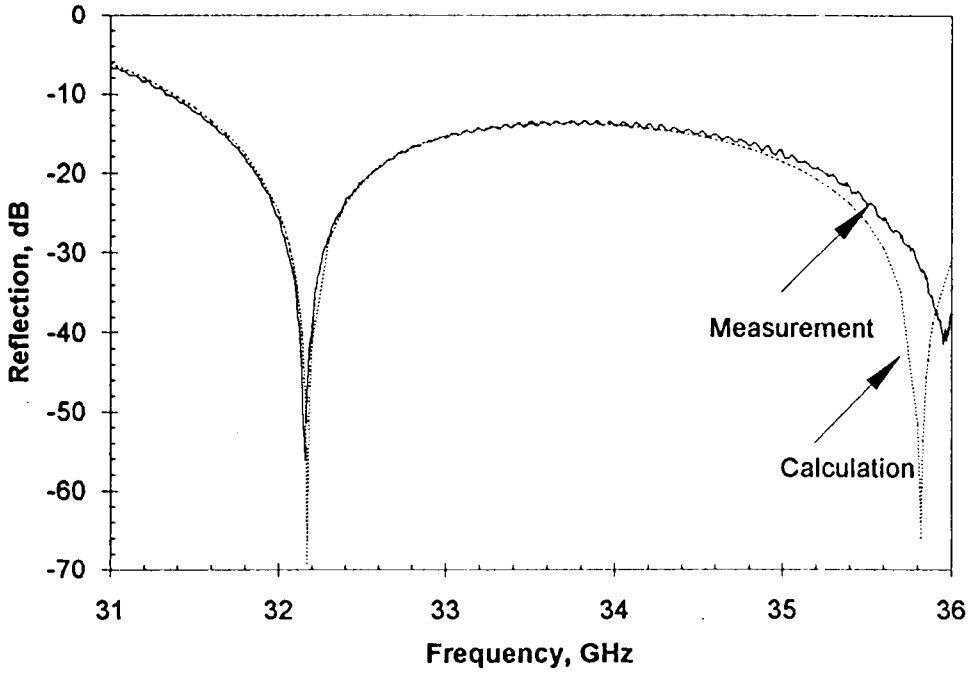
0
-10
-20
-30
-40
-50
-60
-70
Reflection, dB
31
32
33
34
35
36
Frequency, GHz
Measurement
Calculation

Figure 10

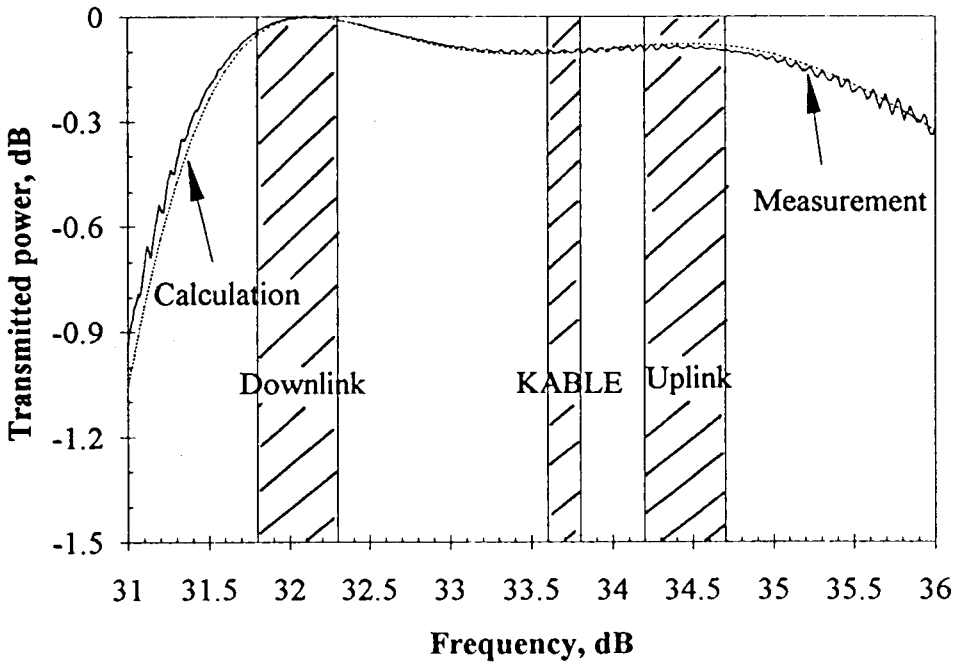
0
-0.3
-0.6
-0.9
-1.2
-1.5
Transmitted power, dB
Calculation
Measurement
Downlink
KABLE
Uplink
31
31.5
32
32.5
33
33.5
34
34.5
35
35.5
36
Frequency, dB

Figure 11

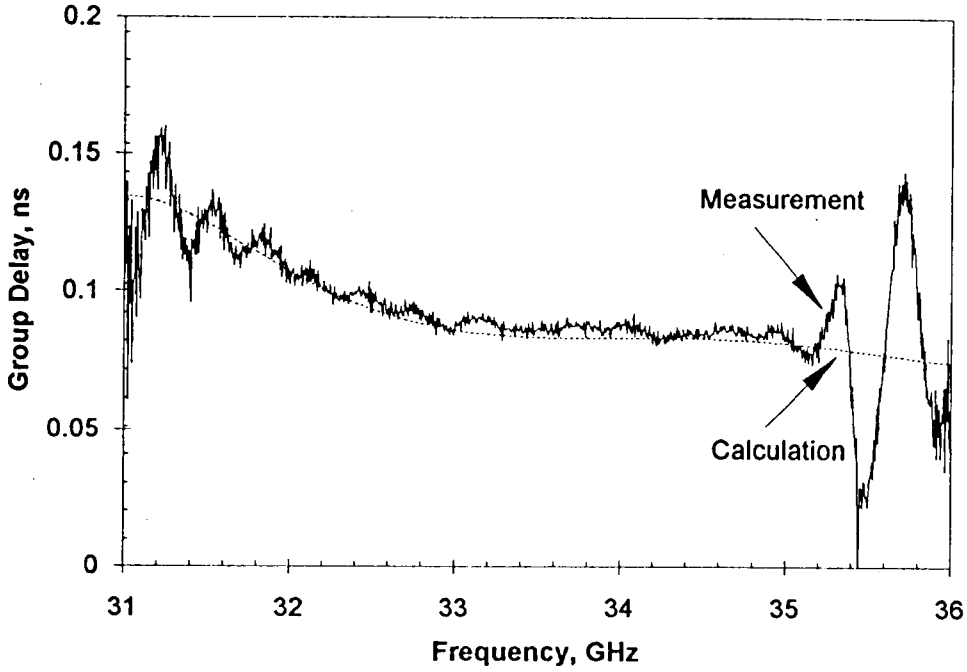
0.2
0.15
0.1
0.05
0
Group Delay, ns
Measurement
Calculation
31
32
33
34
35
36
Frequency, GHz

Figure 12

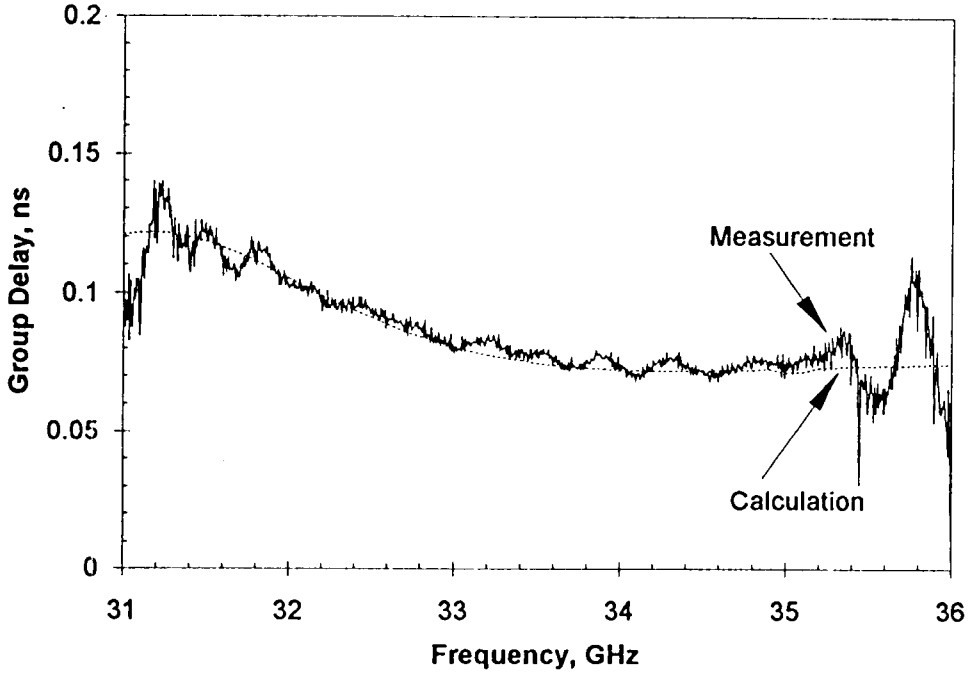
0.2
0.15
0.1
0.05
0
Group Delay, ns
Measurement
Calculation
31
32
33
34
35
36
Frequency, GHz

Figure 13

Figure 10. X/Ka/KABLE dichroic plate installed at DSS-13 beam waveguide antenna